IVYSPRING INTERNATIONAL PUBLISHER

Theranostics

2018; 8(16): 4332-4344. doi: 10.7150/thno.26768

Research Paper

Aptamer-functionalized nanoscale metal-organic frameworks for targeted photodynamic therapy

Hong-Min Meng[1*], Xiao-Xiao Hu[2*], Ge-Zhi Kong[2], Chan Yang[2], Ting Fu[2], Zhao-Hui Li[1]✉, and Xiao-Bing Zhang[2]✉

1. Henan Joint International Research Laboratory of Green Construction of Functional Molecules and Their Bioanalytical Applications, College of Chemistry and Molecular Engineering, Zhengzhou University, Zhengzhou 450001, P. R. China.
2. Molecular Sciences and Biomedicine Laboratory, State Key Laboratory for Chemo/Biosensing and Chemometrics, College of Chemistry and Chemical Engineering, Collaborative Innovation Center for Chemistry and Molecular Medicine, Hunan University, Changsha 410082, P. R. China.

* Authors contributed equally to this work

✉ Corresponding authors: zhaohui.li@zzu.edu.cn; xbzhang@hnu.edu.cn

Received: 2018.04.19; Accepted: 2018.06.30; Published: 2018.07.30

Abstract

Photodynamic therapy (PDT) has been applied in clinical cancer treatment. Here we report an aptamer-functionalized nanoscale metal-organic framework for targeted PDT. Our nanosystem can be easily prepared and successfully used for targeted PDT with a significantly enhanced therapeutic efficacy *in vitro* and *in vivo*.

Methods: By combining the strong binding ability between phosphate-terminated aptamers and Zr-based nanoscale metal-organic frameworks (Zr-NMOFs) and the intercalation of photosensitizer TMPyP4 within the G-quadruplex DNA structure, TMPyP4-G4-aptamer-NMOFs were prepared. The characteristics and photodynamic performance of TMPyP4-G4-aptamer-NMOFs were examined after preparation. Then, we studied their stability, specific recognition ability, and phototoxicity *in vitro*. For *in vivo* experiments, the nanosystem was intratumorally injected into a HeLa subcutaneous xenograft tumor mouse model. After irradiation on day 0, mice were further injected with the nanosystem on day 5 and were again subjected to laser irradiation for 30 min. Tumor volumes and body weights of all mice were measured by caliper every 2 days after the treatment.

Results: The nanosystem induced 90% cell death of targeted cells. In contrast, the control cells maintained about 40% cell viability at the same concentration of nanosystem. For the *in vivo* experiments, the nanosystem-treated group maintained more than 76% inhibition within the entire experimental period.

Conclusion: We have demonstrated that our smart TMPyP4-G4-sgc8-NMOFs nanosystem can be used for targeted cancer therapy with high efficiency.

Key words: nanoscale metal-organic frameworks, aptamer, G-quadruplex, TMPyP4, photodynamic therapy

Introduction

Metal-organic frameworks (MOFs), constructed from metal ions/clusters and organic linkers, are a class of highly ordered crystalline porous materials, and have been applied mostly to applications in catalysis, molecule adsorption and separation as well as sensing due to their large surface area, tunable pores and intriguing functionalities [1, 2]. Since the emergence of nanoscale-MOFs (NMOFs), increasing attention has been paid to the application of NMOFs in biomedical imaging and cancer therapy. Among the large family of NMOFs, Zr-based NMOFs have attracted much interest in recent years because of their outstanding stability, good biocompatibility, and ability to protect nucleic acids from nuclease digestion as well as their intrinsical biodegradability [3-5].

Recently, Lin and coworkers, employed covalent conjugation of fluorescein (FITC) to ligand molecules of Zr-NMOFs for intracellular pH sensing in living

cells [6]. They also use Zr-NMOFs as nanocarriers for the co-delivery of cisplatin and siRNAs to the tumor site for synergistic cancer therapy [7]. Shi and coworkers theranostically used Zr-NMOFs to deliver alendronate to cancer cells [8]. However, most of these nanosystems are based on passive targeting, which is often referred to as the enhanced permeability and retention (EPR) effect. Although the EPR effect can selectively deliver anticancer drugs to tumor sites and improve therapeutic effect, they can only be applied to solid tumors [9], and depend on the leaky nature of the tumor vasculature and prolonged circulation of nano-sized agents, which results in slow and uneven accumulation in the tumor bed [10]. To overcome these limitations, biomarker-targeting ligands, such as antibodies, aptamers, and peptides, have been used to further improve the passive targeting systems. Active targeting, which is achieved by integrating biomarker-targeting ligands into the nanocarrier, can promote cellular uptake at the tumor sites. And it also can specifically deliver drugs to cancer cells more quickly on non-solid tumor sites. Even though several folic acid-integrated MOFs nanosystems have been developed for targeted cancer therapy [11, 12], the preparation of these nanosystems are tedious and very time-consuming. Therefore, it is imperative to develop a highly specific targeted nanosystem that can be synthesized with ease, has high biocompatibility, and is capable of self-delivery (the nanosystem can realize intracellular delivery by themselves with the help of biomarker-targeting ligands) with high efficiency.

Aptamers, which are single-stranded DNA or RNA molecules with specific recognition abilities to their targets [13, 14], have recently attracted significant attention in the field of early diagnosis and cancer therapy based on their numerous advantages. Aptamers have high affinity, high specificity, low toxicity and little immunogenicity with small size and stable structures that are easy to chemically modify [15-17]. Therefore, the combination of aptamers and NMOFs can be employed to deliver drugs selectively to a targeted tumor with high efficiency. It has been well documented that the Zr-O nodes in Zr-NMOFs serve as specific anchors for the effective capture of phosphonates, relying on the strong coordination between the Zr atom and the phosphonate O atoms [3, 18-20]. Therefore, phosphate-terminated aptamers can be efficiently assembled on the surface of Zr-NMOFs for constructing targeted drug delivery systems.

Photodynamic therapy (PDT) has been proved to be one of the most promising and minimally invasive methods for clinical cancer treatment [21-24]. Currently, several photosensitizers have been employed as promising and attractive tools for cancer therapy. These include chlorin e6 (Ce6) [25, 26] and 5, 10, 15, 20-tetrakis (1-methylpyridinium-4-yl) porphyrin (TMPyP4) [27]. Recently, a combination of aptamers and nanocarrier has been used as an efficient delivery strategy for these photosensitizers (Ce6 and TMPyP4) in targeting cancer cells [1, 28, 29].

In this paper, we report for the first time aptamer-functionalized Zr-NMOFs for targeted bioimaging and targeted photodynamic therapy. As shown in **Figure 1**, DNA containing an aptamer and a guanine-rich DNA segment forming a G-quadruplexe structure, herein referred to as G4-aptamer, was synthesized. The G4-aptamer not only loads the photosensitizer (TMPyP4) but also specifically recognizes target cells. Based on the strong complexation of Zr-O-P bonds, the phosphate-functionalized G4-aptamer was easily conjugated to Zr-NMOFs. Once the nanoplatform is delivered into cancer cells via the guiding aptamer, upon light irradiation, the TMPyP4 is activated, generating sufficient reactive oxygen species (ROS) to efficiently kill cancer cells. The whole preparation process is very simple and convenient. Our experimental results showed that our proposed nanosystem could selectively bind to target cells and act as a photosensitizer carrier with high efficiency.

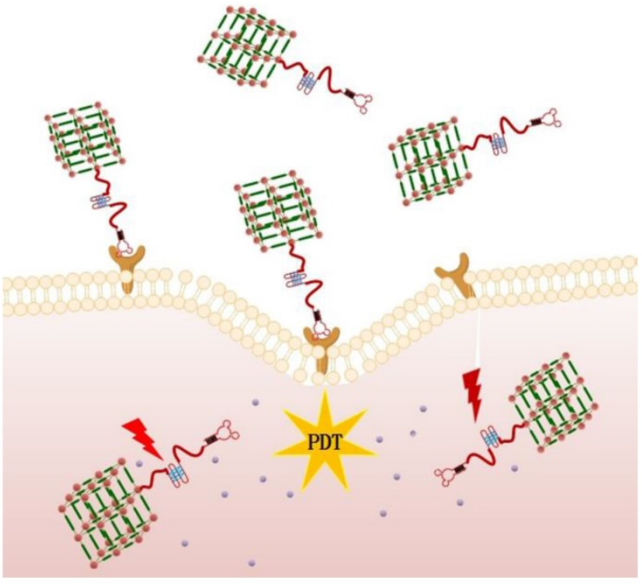

Figure 1. Schematic representation of aptamer-targeted delivery of TMPyP4-G4-aptamer-NMOFs nanosystem for PDT in living cells.

Results and discussion

Preparation and characterization of Zr-NMOFs

Zr-NMOFs were synthesized by a traditional solvothermal reaction between $ZrCl_4$ and H_2BDC in N, N-dimethylformamide (DMF) at 90 °C for 18 h.

Transmission electron microscopy (TEM) (**Figure 2A**), dynamic light scattering (DLS) (**Figure 2B**) and X-ray photoelectron spectroscopy (XPS) (**Figure 2C**) were used to analyze the morphology of Zr-NMOFs. It was observed that the nanoparticles were monodisperse with an average particle size of 93 nm with a polydispersity index of 0.132±0.003.

Stability assay of Zr-NMOFs

Stability of a nanocarrier is a crucial factor to be taken into account in the design of a drug delivery system. The stability of Zr-NMOFs in biological media was confirmed by TEM after culturing the nanoparticles in DMEM cell culture medium and cell lysate for 8 h. As shown in **Figure 2D-E**, the morphology of Zr-NMOFs did not obviously change. Powder X-ray diffraction (PXRD) results were also used to investigate the stability of Zr-NMOFs in biological media. The nanoparticles retained their crystallinity after 24 h incubation with Tris buffer (**Figure 2F**). These results suggest that the Zr-NMOFs nanoparticles have sufficient stability and can be used as nanocarriers for drug delivery.

Preparation and characterization of TMPyP4-G4-aptamer-NMOFs nanosystem

TMPyP4-G4-aptamer-NMOFs nanosystem was synthesized by reacting Zr-NMOFs with phosphate-functionalized G4-aptamer to fabricate the G4-aptamer-NMOFs. In our design, sgc8, which can specifically bind to the cellular membrane receptor protein tyrosine kinase 7 (PTK7), a protein highly expressed on HeLa (human cervical cancer) cells and human leukemia CEM cells, was chosen as the model aptamer. The synthesis processes were monitored by Zeta potential and gel electrophoresis experiments. The surface Zeta potentials of Zr-NMOFs and G4-sgc8-NMOFs were 3.0 and -5.5 mV, respectively. The binding between G4-sgc8 and Zr-NMOFs was further validated using nitrogen adsorption measurements. The Brunauer-Emmett-Teller (BET) model was adopted to calculate the surface area of Zr-NMOFs and G4-sgc8-NMOFs. As shown in **Figure S1A**, the specific surface area of G4-sgc8-NMOFs was significantly larger than that of Zr-NMOFs. This observation indicates that G4-sgc8-NMOFs can prevent strong interparticle interaction for better dispersibility. The pore size distribution of the products was obtained by the Barret-Joyner-Halenda (BJH) model (**Figure S1B**).

Because NMOFs can protect nucleic acids from nuclease digestion, gel electrophoresis experiments were then carried out under different conditions. As shown in **Figure S2**, a G4-sgc8 band was clearly visible upon incubating G4-sgc8-NMOF in serum for up to 8 h, while the naked G4-sgc8 was completely degraded under the same condition. This result intimates that the Zr-NMOFs-based delivery system showed greater stability against enzymatic digestion than that shown by the monomeric DNA-based system. This observation favors the application of our nanosystem to *in vivo* applications. The efficiency of

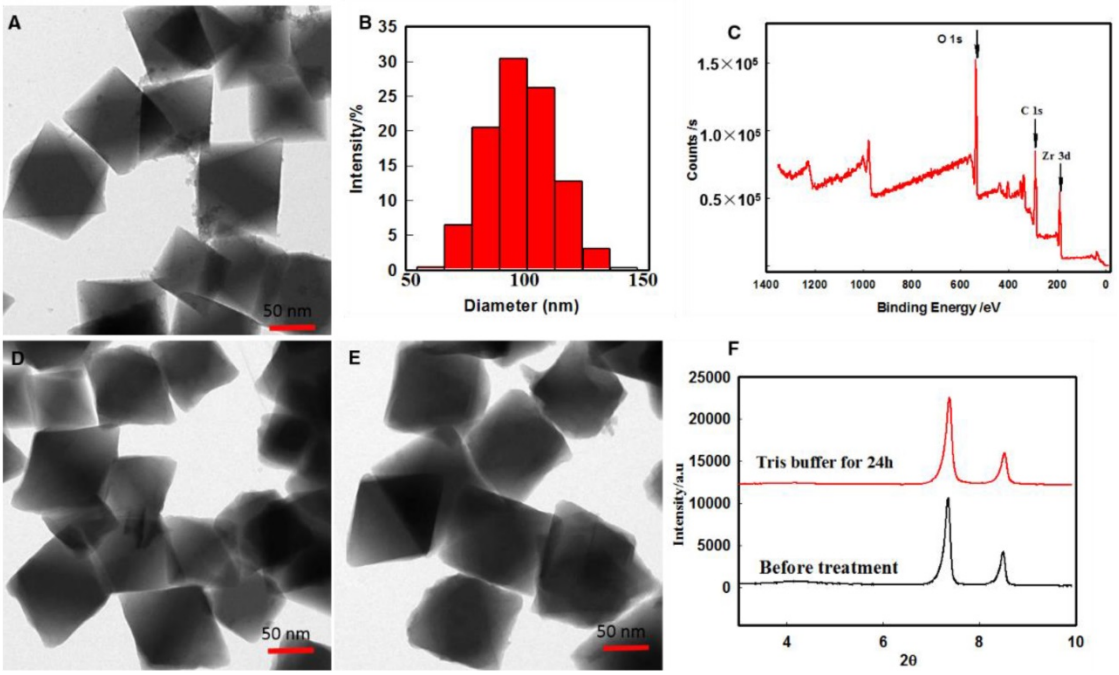

Figure 2. Morphology and structure of Zr-NMOFs.(A)TEM image of Zr-NMOFs. **(B)**DLS of Zr-NMOFs (PDI=0.132). **(C)**XPS of Zr-NMOFs. **(D)**TEM image of Zr-NMOFs after DMEM cell culture medium cultivation. **(E)**TEM image of Zr-NMOFs after cell lysate cultivation. **(F)** PXRD patterns of Zr-NMOFs, and Zr-NMOFs after incubating in Tris buffer for 24 h.

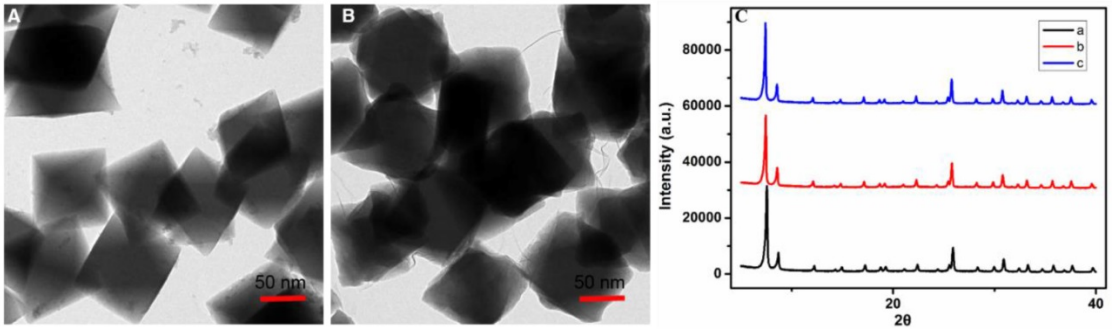

Figure 3. Morphology and structure of TMPyP4-G4-sgc8-NMOFs. (A) TEM image of TMPyP4-G4-sgc8-NMOFs. **(B)** TEM image of TMPyP4-G4-sgc8-NMOFs after incubating in PBS buffer (pH 6.0) for 8 h. **(C)** PXRD patterns of (a) Zr-NMOFs, (b) TMPyP4-G4-sgc8-NMOFs and (c) TMPyP4-G4-sgc8-NMOFs after incubating in PBS buffer (pH 6.0) for 8 h.

the assembled G4-sgc8-NMOF was estimated to be 94.2% by measuring the absorbance at 260 nm. These results indicated that the surface of the Zr-NMOFs nanoparticles was successfully coated by the G4-sgc8 with a high efficiency.

In this study, we choose TMPyP4 as photosensitizer for PDT. Due to its unique symmetrical aromatic structure and cationic properties, TMPyP4 can bind to and stabilize the G-quadruplex structure. In this study, TMPyP4 was used as a photosensitizer for PDT due to its unique symmetrical aromatic structure and cationic properties. These properties of the photosensitizer enabled it to bind and stabilize the G-quadruplex structure. The binding mechanism is that TMPyP4 could recognize G-quadruplex structure and then bond with two G-quadruplexs. The G-quadruplex-TMPyP4 composite shown in a space-fill mode and a relatively lower energy [30].

A large complex (G4-sgc8-NMOFs) was successfully formed after mixing G4-sgc8 with TMPyP4. The binding interaction between TMPyP4 and G4-sgc8 was confirmed by Fourier-transform infrared (FTIR) spectroscopy (**Figure S3**). The band observed at 1112 cm^{-1}, confirmed the presence of a phosphate group. Circular dichroism (CD) spectroscopy also indicated the formation of the TMPyP4-G4-sgc8 complex. As shown in **Figure S4**, a new negative peak appeared between 400 and 450 nm, indicating a mixed binding mode of TMPyP4 to G4-sgc8.

The absorbances of TMPyP4-G4-sgc8 and TMPyP4-G4-sgc8-NMOFs were recorded by UV-vis spectrophotometry to study the interactions among TMPyP4, G4-sgc8 and Zr-NMOFs. **Figure S5A** shows the changes in intensity and location of TMPyP4 when mixed with G4-sgc8. A red shift from 422 to 436 nm was observed with the addition of G4-sgc8 to the TMPyP4 solution. To investigate the formation of TMPyP4-G4-sgc8-NMOFs, the UV/Vis spectra of G4-sgc8, Zr-NMOFs and TMPyP4-G4-sgc8-NMOFs were also measured. As shown in **Figure S5B,** the absorption peaks of G4-sgc8-Zr-NMOFs and TMPyP4-G4-sgc8 were recorded at 242 nm and 436 nm respectively, demonstrating the successful assembly of the nanosystem.

Having confirmed the successful assembly of our design, the morphology and stability of the TMPyP4-G4-sgc8-NMOFs were then examined. TEM of TMPyP4-G4-sgc8-NMOFs revealed an octahedron structure similar to that of Zr-NMOF (**Figure 3A**). The stability of TMPyP4-G4-sgc8-NMOFs in biological media was confirmed after culturing the nanosystem in 10 mM PBS buffer solution at pH 6.0 for 8 h. From **Figure 3B**, there was a slight change in the morphology of the NMOFs. PXRD data also confirmed that the TMPyP4-G4-sgc8-NMOFs nanosystem retained its crystallinity in buffer for 8 h (**Figure 3C**). These results suggest that the nanosystem remained intact as MOF until PDT treatment, considering typical cellular internalization and irradiation time for the treatment.

Specific recognition ability of the nanosystem

We then evaluated the specific recognition ability of G4-sgc8-NMOFs to target cancer cells by flow cytometry and confocal microscopy. In order to give a visible signal, FITC fluorophore was modified at the 3'-terminal of G4-sgc8. After incubating with G4-sgc8-NMOFs or G4-sgc8 for 0.5 h, we recorded the fluorescence signal of HeLa cells (positive cells), CEM cells (positive cells) and Ramos cells (negative cells). As shown in **Figure 4A-C**, a significant signal shift was observed for HeLa and CEM cells treated with G4-sgc8-NMOFs or G4-sgc8. However, no obvious fluorescence signal change was observed in the Ramos cells. In order to further investigate the specific recognition ability of G4-sgc8-NMOFs, a random library (lib) sequence was chosen as a control. From the results, it was observed that lib-NMOFs gave a weak signal, as recorded for untreated cells. These results indicated that G4-sgc8-NMOFs could maintain

its specific binding ability to target cells. Furthermore, confocal imaging of G4-sgc8-NMOFs was also investigated. From **Figure 4D**, the HeLa cells treated with G4-sgc8-NMOFs for 4 h showed strong fluorescence signals in cytoplasm. However, the Ramos cells, which were subjected to the same treatment showed weak fluorescence (**Figure S6**), which is in good agreement with the results of flow cytometry. These results suggest that this nanosystem could maintain specific binding ability to target cells and could be used to deliver photosensitizer into target cells for PDT.

Evaluation of SOG

Because PDT utilizes singlet oxygen to kill cancer cells, the efficient generation of singlet oxygen is critical for a new theranostic nanosystem with PDT function. The singlet oxygen generated by this nanosystem was evaluated by singlet oxygen sensor green (SOSG), which can be specifically oxidized by singlet oxygen to produce enhanced fluorescence. As shown in **Figure S7**, the fluorescence emission intensity of SOSG increased by 3.8-, 4.3- and 6.0-fold in 50 min when the nanosystem was irradiated by 405 nm laser (2 W/cm^2), white light (with a wavelength ranging from 400 nm to 700 nm and power density of 2.82 W/cm^2) and 660 nm laser (2 W/cm^2), respectively. This observation suggested that singlet oxygen was efficiently produced by the TMPyP4-G4-sgc8-NMOFs nanosystem.

We also investigated the singlet oxygen generated by TMPyP4-NMOFs, which was obtained by directly loading TMPyP4 into the pores of MOFs. The TMPyP4-NMOFs nanosystem presented much lower SOSG fluorescence intensity than that of TMPyP4-G4-sgc8-NMOFs (**Figure S8**), demonstrating that self-quenching could efficiently inhibit SOG from TMPyP4 outside the cells and, hence, limit the side effects of PDT.

Phototoxicity investigation of the nanosystem

To identify the selective phototoxicity of the TMPyP4-G4-sgc8-NMOFs nanosystem, the MTS assay (MTS = 3-(4, 5-dimethylthiazol-2-yl)-5-(3-carboxy-methoxyphenyl)-2-(4-sulfophenyl)-2-H-tetrazolium) was conducted on both target HeLa and CEM cells and non-target Ramos cells. In this assay, all cells were treated with free TMPyP4 and TMPyP4-G4-sgc8-NMOFs nanosystem. As shown in **Figure 5A-C**, TMPyP4-G4-sgc8-NMOFs induced 91.3% and 90.1% cell death for targeted HeLa cells and CEM cells, respectively. In contrast, the Ramos cells maintained about 40% cell viability at a concentration of 5 μM. However, at the same concentration of TMPyP4, free TMPyP4 showed minimal cytotoxicity with cell viabilities of 60.8%, 61.3% and 62.3% for HeLa, CEM and Ramos cells, respectively. This demonstrates the robust cytotoxic efficacy of TMPyP4-G4-sgc8-NMOFs in target cells and the excellent selective cytotoxicity of this molecular drug transported by G4-sgc8-NMOFs. In order to further investigate active targeting upon sgc8 modification, TMPyP4-G4-lib-MOFs was introduced as control. From the results, it was ascertained that the HeLa cells, CEM cells and Ramos cells could maintain 38.2%, 43.8% and 39.1% cell viability after treatment

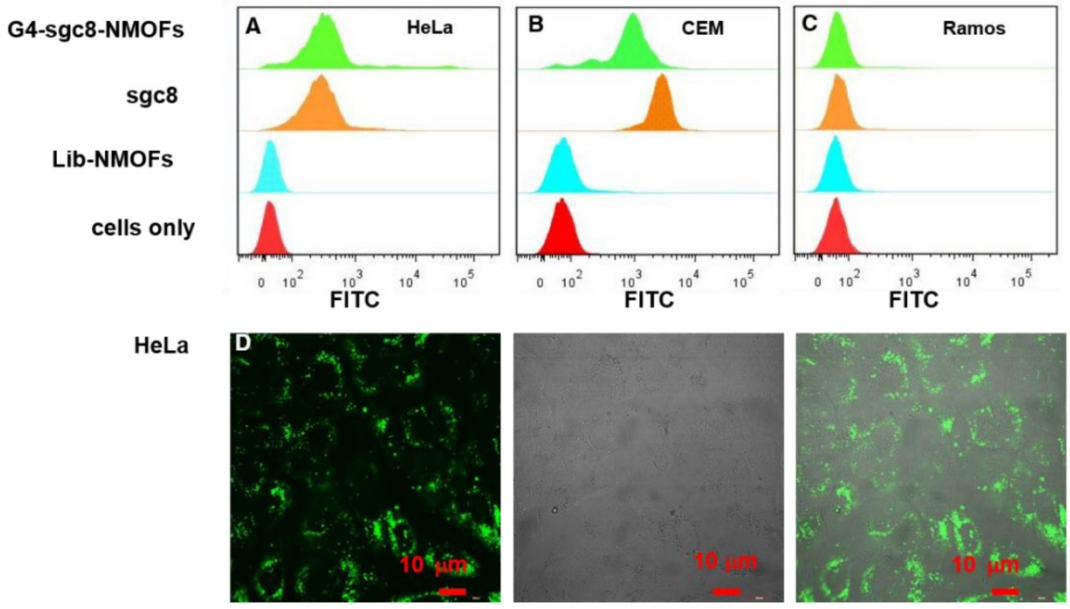

Figure 4. Flow cytometry analysis and confocal microscopy imaging of TMPyP4-G4-sgc8-NMOFs nanosystem. (A) HeLa cells, **(B)** CEM cells and **(C)** Ramos cells. (D) Confocal laser-scanning microscopy imaging of HeLa cells treated with the nanosystem. Cells were incubated with 100 μg/mL of G4-sgc8-NMOFs.

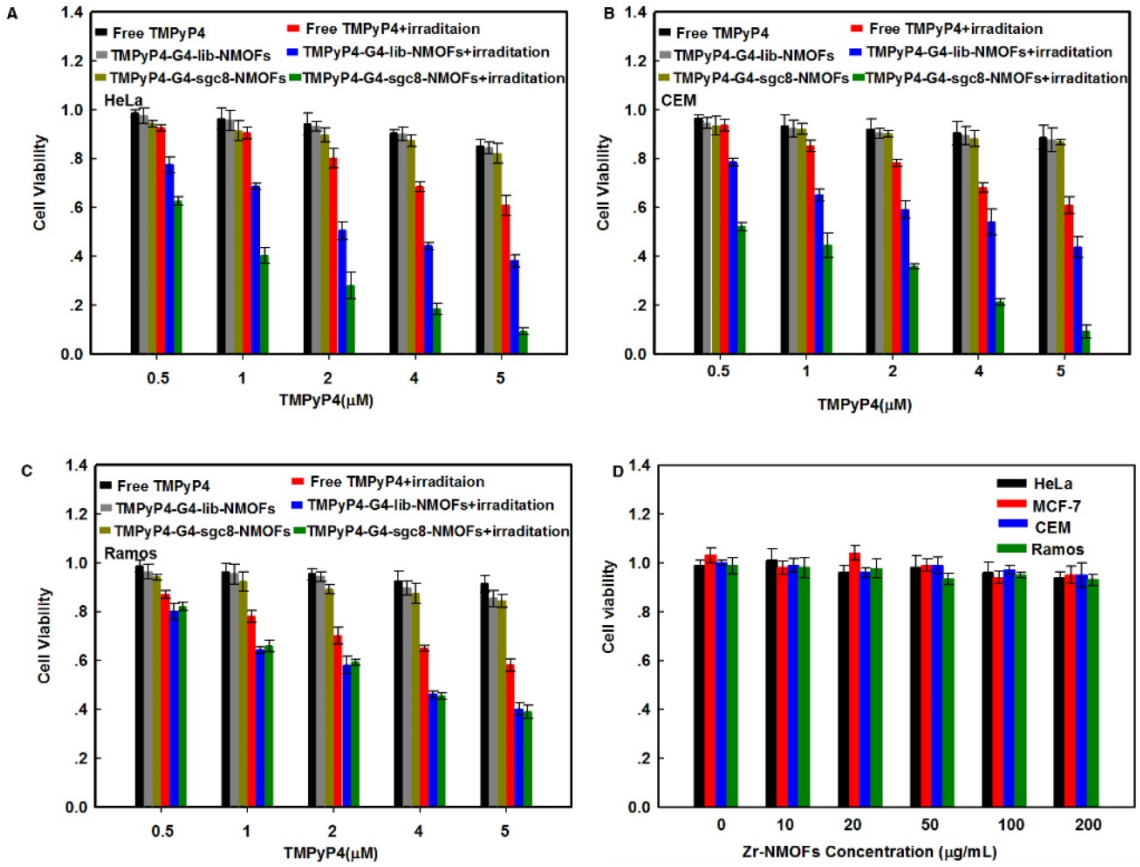

Figure 5. Phototoxicity assay of the nanosystem. Cell viability of free TMPyP4 (red bar), TMPyP4-G4-lib-NMOFs (blue bar), and TMPyP4-G4-sgc8-NMOFs nanosystem (green bar) on **(A)** HeLa cells, **(B)** CEM cells and **(C)** Ramos cells under different conditions as indicated. **(D)** Cytotoxicity of Zr-NMOFs on cancer cells under different conditions.

with TMPyP4-G4-lib-NMOFs at a concentration of 5 μM TMPyP4. These results demonstrated that the TMPyP4-G4-sgc8-NMOFs nanosystem was much more efficient than TMPyP4-G4-lib-NMOFs. It was observed that in the absence of irradiation, the cancer cells exhibited high viability when incubated with the nanosystems (TMPyP4, TMPyP4-G4-lib-NMOFs and TMPyP4-G4-sgc8-NMOFs), indicating that the therapeutic effect was highly light dependent.

Moreover, low cytotoxicity was observed for Zr-NMOFs at concentrations up to 200 μg/mL, with cell viabilities of 94.1%, 95.0%, 94.8% and 93.5% for HeLa, MCF-7, CEM and Ramos cells, respectively (**Figure 5D**).

PDT of the TMPyP4-G4-sgc8-NMOFs nanosystem was much more efficient than that of TMPyP4-G4-sgc8 at the same concentration of TMPyP4 for both target cells and non-target cells (**Figure S9**). This result proved that NMOFs play a nanocarrier role in TMPyP4-G4-sgc8-NMOFs-induced phototoxicity. All these results demonstrated that the G4-sgc8 coating on the nanocarriers could be used for targeted PDT and TMPyP4-G4-sgc8-NMOFs could enhance TMPyP4 uptake and result in remarkably increased PDT efficacy.

To further investigate the therapeutic effectiveness of the TMPyP4-G4-sgc8-NMOFs to cancer cells, real-time monitoring was performed. Both HeLa and Ramos were first incubated with TMPyP4-G4-sgc8-NMOFs for 4 h and then irradiated using the confocal microscope. As shown in **Figure 6A**, after 4 min irradiation (405 nm laser, 2 W/cm^2), the red fluorescence in HeLa cells gradually decreased. At the same time, the HeLa cells began to swell, and more bubbles appeared on the surface of the cells, which resulted in the rupture of the outer membrane (**Figure 6B**), while morphological changes to Ramos cells occurred after 15 min irradiation (**Figure S10A**). The morphology of HeLa cells that were only treated with irradiation did not significantly change (**Figure S10B**). These results suggested that the TMPyP4-G4-sgc8-NMOFs nanosystem provided specific cytotoxicity to target cancer cells.

The feasibility of *in vivo* PDT using TMPyP4-G4-sgc8-NMOFs was then verified by investigating the fate of TMPyP4 using fluorescence imaging assay on a HeLa subcutaneous xenograft tumor mouse model. After intratumoral injection, fluorescence intensity of TMPyP4 increased in the first 2 h and then

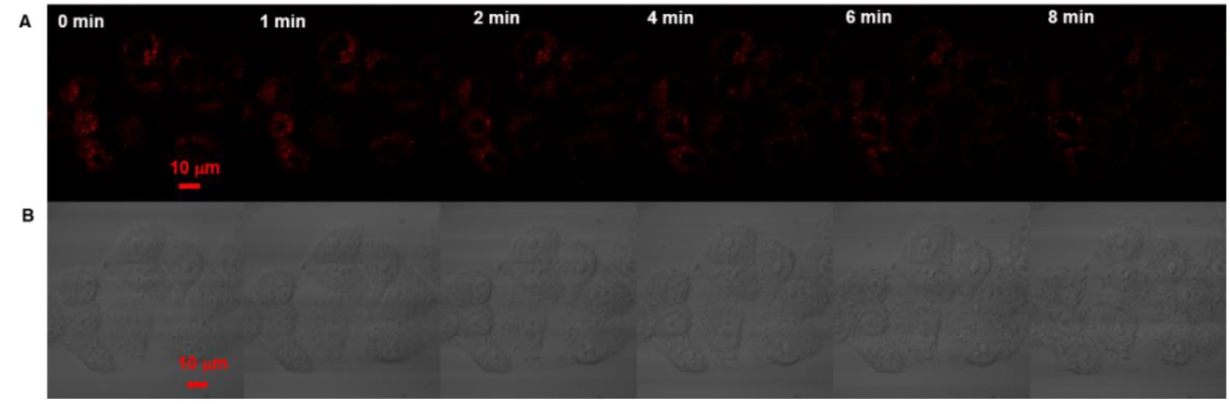

Figure 6. Confocal imaging assay of therapeutic effectiveness to HeLa cells. (A) Real-time fluorescence images and morphology of HeLa cells treated with TMPyP4-G4-sgc8-NMOFs nanosystem and laser at 405 nm. **(B)** Bright-field images.

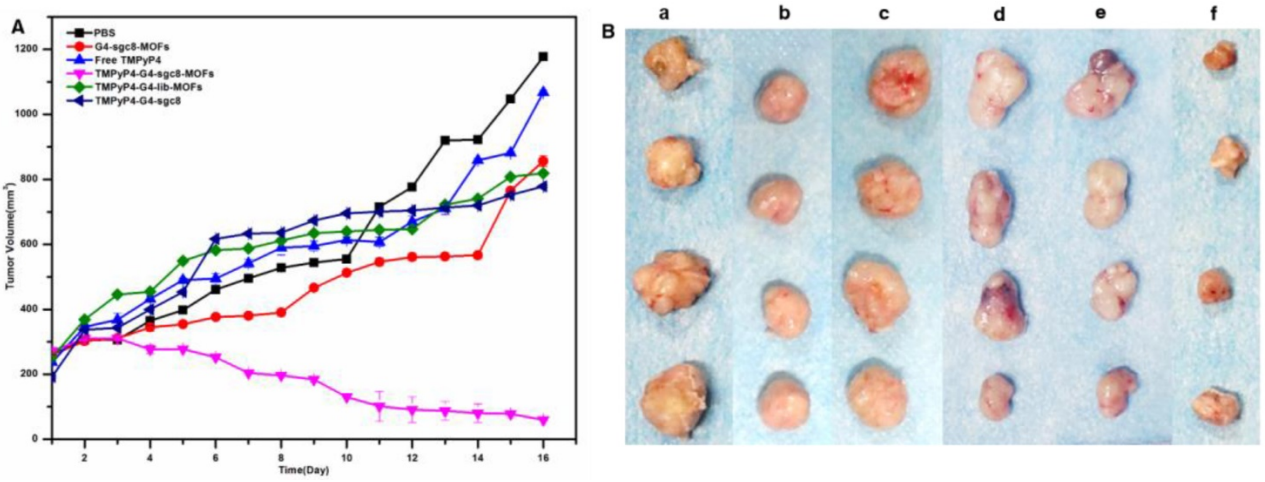

Figure 7. *In vivo* efficacy of PDT on HeLa tumor-bearing mice. (A) Tumor growth inhibition curve after PDT treatment. **(B)** Photos of tumors of each group after PDT. (a) PBS, (b) G4-sgc8-NMOFs, (c) free TMPyP4, (d) TMPyP4-G4-lib-NMOFs, (e) TMPyP4-G4-sgc8, (f) TMPyP4-G4-sgc8-NMOFs. P values were calculated by *t*-test; ** P<0.01.

decreased gradually. The decreased fluorescence most likely resulted from the spread of TMPyP4 throughout the animal's body. Thus, the best timing for PDT is 2 h after intratumoral injection (**Figure S11**).

Then, we evaluated the *in vivo* PDT efficacy of the TMPyP4-G4-sgc8-NMOFs platform. The mice were treated with PBS as control, G4-sgc8-NMOFs, free TMPyP4, TMPyP4-G4-lib-NMOFs, TMPyP4-G4-sgc8 and TMPyP4-G4-sgc8-NMOFs by intratumoral injection. Experimental results (**Figure 7A**) showed that an obvious tumor-growth inhibition was achieved in the group treated with the TMPyP4-G4-sgc8-NMOFs as their tumor size reduced drastically from 250 mm^3 to 59.7 mm^3 (~76%). Tumor growth was slightly inhibited by NMOFs-sgc8 in the first 8 days, after which a rapid recovery of tumor growth was observed, while the TMPyP4-G4-sgc8-NMOFs group maintained more than 76% inhibition within the entire experimental period (16 days after treatment). The representative tumor and mouse images are shown in **Figure 7B** and **Figure 8**, respectively.

In contrast, the tumors of mice treated with either PBS (1177.4 mm^3) or free TMPyP4 grew rapidly, which is consistent with previous findings that free TMPyP4 at such a low dose is not effective in inhibiting tumor growth. TMPyP4-G4-sgc8-NMOFs was more efficient than free TMPyP4 in treating the tumors. The effectiveness of TMPyP4-G4-sgc8-NMOFs could be attributed to its novel characteristics. TMPyP4-G4-sgc8-NMOFs showed specific targeting ability and had a larger molecular weight. Once TMPyP4-G4-sgc8-NMOFs was injected into the tumor site, TMPyP4 was quickly delivered into cancer cells via the guiding sgc8. These characteristics enabled it to accumulate a relatively higher concentration of the drug in the mouse tumor and a longer drug retention time. In contrast, free TMPyP4 might be cleared away from the tumor site before irradiation. Histology of frozen tumor, liver and kidney slices also confirmed that TMPyP4-G4-sgc8-NMOFs treatment caused significant apoptosis/necrosis of tumors (**Figure 9**).

During the experimental period, the body weights and organs coefficients of the mice were

monitored. The organ coefficient was the value of organ weight / body weight ratio, which was a basic data to evaluate the effect of nanosystem on organ of the mouse. There are no significant weight variation upon different treatments, as shown in **Figure 10 A**. Meanwhile, no obvious changes of organ coefficient were observed for heart, liver, spleen, lung, kidney and stomach when they were treated with different conditions (**Figure 10 B**). All these results further confirmed the very low toxicity of G4-sgc8-NMOFs *in vivo* at our tested doses. Overall, these data demonstrated the potent antitumor efficacy and delivered via G4-sgc8-NMOFs.

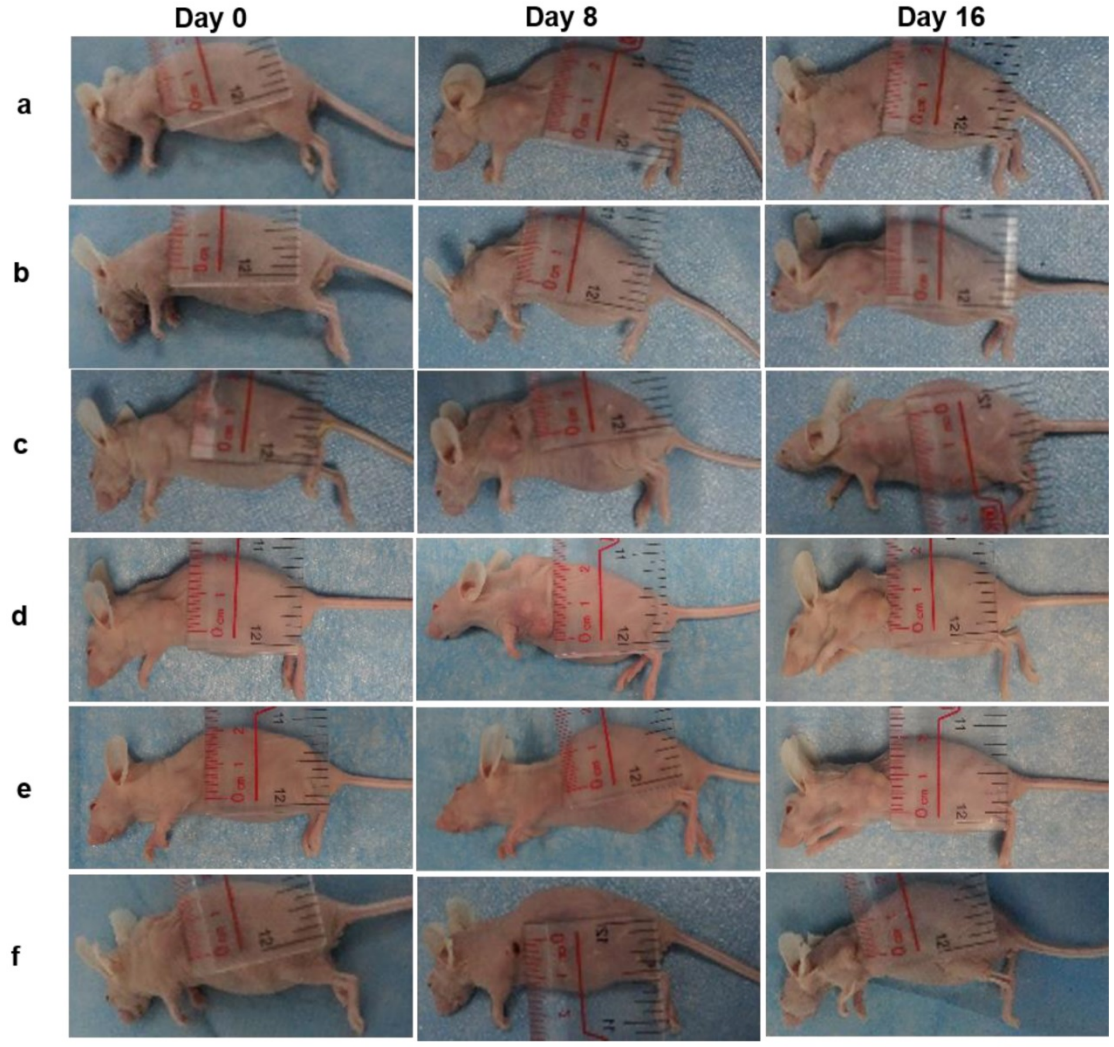

Figure 8. *In vivo* efficacy of PDT on HeLa tumor-bearing mice. Photos of mice on Day 0, Day 8 and Day16. (a) PBS, (b) G4-sgc8-NMOFs, (c) free TMPyP4, (d) TMPyP4-G4-lib-NMOFs, (e) TMPyP4-G4-sgc8, (f) TMPyP4-G4-sgc8-NMOFs.

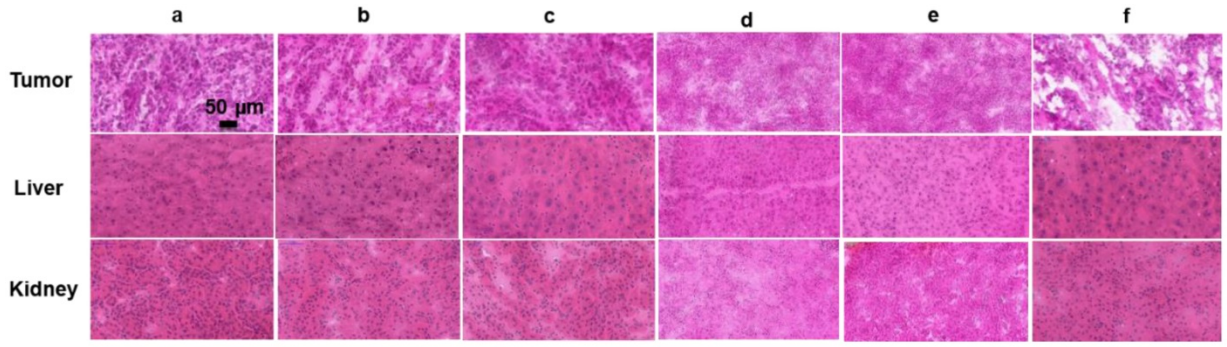

Figure 9. Histology of tumor, liver and kidney slices collected from different groups of mice 16 days post-treatment. (a) PBS, (b) G4-sgc8-NMOFs, (c) free TMPyP4, (d) TMPyP4-G4-lib-NMOFs, (e) TMPyP4-G4-sgc8, (f) TMPyP4-G4-sgc8-NMOFs.

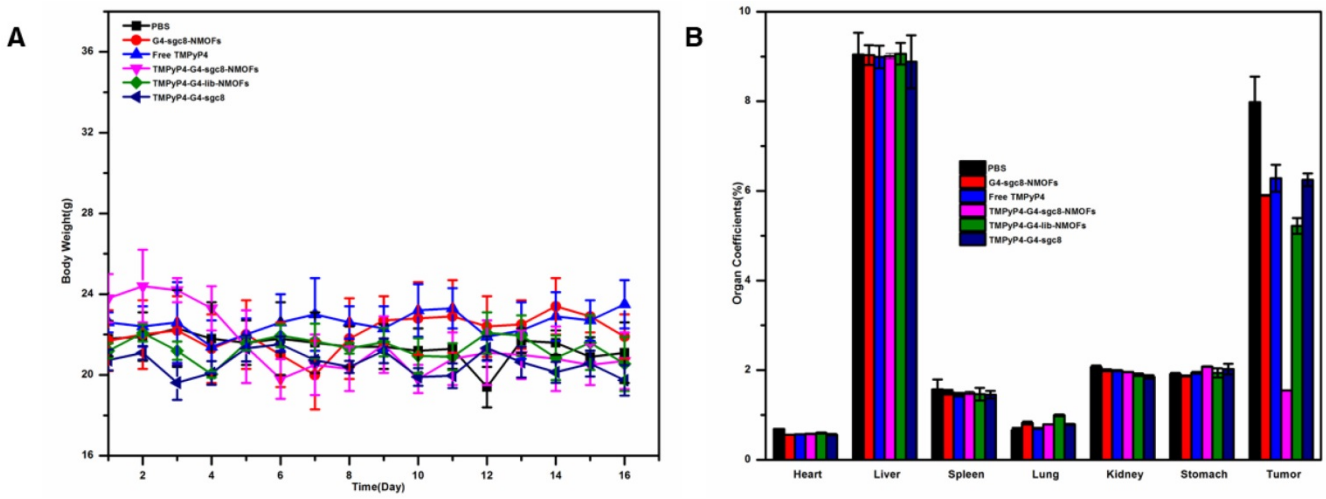

Figure 10. The body weight and organ coefficients of different mice groups. (A) The body weight changes of mice bearing HeLa tumors. **(B)** Organ coefficients of mice bearing HeLa tumors. Each bar represents the mean ± SD. Mice were euthanized when tumors reached ~1200 mm³ in size (n=4 for each group).

Conclusion

In summary, we developed a smart cancer-specific imaging and photodynamic therapy system by conjugating cell-specific aptamer as a targeting domain and G-quadruplex as photosensitizer carrier domain onto Zr-NMOFs surface through strong Zr-O-P bonds. The TMPyP4-G4-sgc8-NMOFs nanosystem we developed possesses the following unique features: high TMPyP4 loading efficiency, enhanced delivery of TMPyP4 into target cells and targeted PDT *in vivo*. In addition, the NMOFs also show high stability, good biocompatibility, and the ability to protect nucleic acids from nuclease digestion, indicating its potential application in biomedical research. Therefore, this smart TMPyP4-G4-sgc8-NMOFs nanosystem can be explored further as a multifunctional treatment tool for early diagnosis and targeted cancer therapy.

Methods

Materials

DNA oligonucleotides used in this work were synthesized and purified by Sangon Biotechnology Co., Ltd. (Shanghai, China), and their sequences and modifications are listed in **Table S1**. Zirconium chloride ($ZrCl_4$), terephthalic acid (H_2BDC), acetic acid (CH_3COOH), TMPyP4, tRNA were purchased from Sigma-Aldrich and used as received without further purification. Fetal bovine serum, DMEM medium, and penicillin-streptomycin solution were purchased from Invitrogen. All solutions were prepared using ultrapure water, which was prepared using a Millipore Milli-Q water purification system (Billerica, MA, USA), with an electrical resistance >18.3 MΩ.

Cell lines and cell culture

HeLa cells were purchased from ATCC (American Type Culture Collection, Manassas, VA, USA) and incubated in DMEM media supplemented with 10% (v/v) fetal bovine serum and 0.5 mg/mL penicillin-streptomycin at 37 °C in 5% CO_2 atmosphere. CEM (CCL-119, T-cell line, human ALL) and Ramos (CRL-1596, B-cell line, human Burkitt's lymphoma) cells were maintained in RPMI 1640 medium with 10% fetal bovine serum (FBS) and 0.5 mg/mL penicillin-streptomycin at 37 °C under a 5% CO_2 atmosphere. Cells were washed before and after incubation with Dulbecco's phosphate-buffered saline (DPBS). Binding buffer used for flow cytometric analysis was prepared by adding yeast tRNA (0.1 mg/mL) and BSA (1 mg/mL) to the DPBS buffer to reduce background binding.

Tumor model

Athymic nude female mice were obtained from Hunan SLRC Laboratory Animal Co., Ltd. and used under protocols approved by Hunan University Laboratory Animal Center. The HeLa tumor models were generated by subcutaneous injection of 1×10^7 cells in 100 μL PBS into the mice. The mice were used for PDT when the tumor volume reached about 250 mm³.

Instruments

The absorption spectra in this work were collected using a UV-2450 UV-vis spectrophotometer (Shimadzu, Japan). Dynamic light scattering (DLS) was measured using a Malvern Zetasizer Nano ZS90 (Malvern Instruments, Ltd., Worcestershire, UK). Transmission electron microscopy (TEM) was carried out using a JEM-2100 transmission electron

microscope (JEOL, Japan) with a working voltage of 200 kV. The crystal structure was measured using a D 8 Advance X-ray diffractometer (Bruker, Germany). Circular dichroism measurements were collected using a MOS-500 circular dichroism spectrometer (Biologic, Germany). The concentration of cancer cells was determined by a TC10TM automated cell counter (Bio-Rad, USA). Flow cytometry measurements were obtained using a FACScan cytometer (Becton Dickinson, USA). The MTS assay was carried out using a Synergy 2 Multi-Mode Microplate Reader (Bio-Tek, USA). Cell fluorescence images were obtained using a confocal laser-scanning microscope (Olympus FV1000, Japan).

Preparation of Zr-NMOFs

3.0 mg terephthalic acid (H_2BDC) was dissolved in 3 mL of N, N dimethylformamide (DMF). In a separate vial, 3.24 mg zirconium chloride (0.066 mmol) was dissolved in 3 mL of DMF. The two solutions were mixed together in a 10 mL vial, and acetic acid (900 μL) was added to the reaction mixture. The reaction mixture was kept in a 90 °C oven for 18 h to yield Zr-NMOFs. Zr-NMOFs nanoparticles were washed with copious amounts of DMF, 1% triethylamine in ethanol (v/v) and water successively before being dispersed in water for characterization and functionalization with G4-aptamer.

Synthesis of TMPyP4-G4-sgc8-NMOFs nanosystem

First, annealed G4-sgc8 (100 μM) was mixed with different concentrations of TMPyP4 (20, 40, 80, 100, 200, 400 μM) in Tris buffer (pH 7.4, 20 mM Tris, 200 mM KCl) for 30 min. Then, the above complex was added to an aqueous solution of Zr-NMOFs (10 mg/mL) and mixed on a mechanical shaker for 1 h at room temperature. At last, free oligonucleotides and TMPyP4 were removed by centrifugation (10142 ×g, 10 min) three times, followed by resuspension of the TMPyP4-G4-sgc8-NMOF nanosystem in buffer solution for characterization and analysis.

UV absorption titration

Different concentrations (0, 0.05, 0.1, 0.15, 0.2, 0.3, 0.4, 0.5, 0.8, 1.0 μM) of annealed G4-sgc8 in Tris buffer (pH 7.4, 20 mM Tris, 200 mM KCl) were mixed with TMPyP4 (4 μM) at room temperature. After 20 min, the absorption spectra of the mixtures were recorded on a UV-2450 UV-vis spectrophotometer.

Circular dichroism tests

Annealed G4-sgc8 in Tris-HCl buffer (pH 7.4, 20 mM Tris, 200 mM KCl), TMPyP4 in annealed G4-sgc8, and free TMPyP4 were tested using a circular dichroism spectrometer from 200 to 500 nm. The final molar concentration of G4-sgc8 was 10 μM.

Agarose gel electrophoretic experiments

Four samples were prepared for gel electrophoresis. The experiments were performed in 20 μL Tris-HCl buffer solution. The four samples were composed of (1) 10 μM G4-sgc8; (2) 10 μM G4-sgc8-NMOFs; (3) 10 μM G4-sgc8 pretreated with serum for 8 h; (4) 10 μM G4-sgc8-NMOFs pretreated with serum for 8 h. These samples were applied to an agarose gel (2% agarose). The electrophoresis was carried out in 1×TBE buffer (90 mM Tris, 90 mM boric acid, and 10 mM EDTA, pH 8.0) at 100 V for 1.5 h and the gels were stained with ethidium bromide.

Flow cytometry experiments

HeLa cells (4×10^5) were seeded in 30-mm dishes and incubated for 24 h before experiments. After removing the culture medium, cells were washed three times with washing buffer. Subsequently, cells were incubated with 100 nM G4-sgc8, 42.5 μg/mL G4-sgc8-NMOFs (100 nM G4-sgc8) or 100 nM random library sequence in binding buffer at 4 °C for 30 min. The cells were washed three times with washing buffer and then detached with 100 μL of trypsin. Finally, the cells were resuspended in binding buffer (100 μL), and then subjected to flow cytometric analysis by counting 10,000 events. CEM and Ramos cells were also used to flow cytometric analysis. CEM cells (4×10^5) and Ramos cells (4×10^5) were incubated with 100 nM sgc8, 42.5 μg/mL G4-sgc8-NMOFs (100 nM G4-sgc8) or 100 nM random library sequence in a 200 μL volume of binding buffer at 4 °C for 30 min. Then, the cells were washed with washing buffer three times, centrifuged at 45×g for 3 min, and resuspended in binding buffer (100 μL) for flow cytometric analysis. The flow cytometric analysis was performed on a BD FACSVerse™ flow cytometer with a green laser at 494 nm as the excitation source.

Confocal laser-scanning microscopy experiments

HeLa cells (4×10^4) were seeded in 35-mm confocal dishes and incubated for 24 h. After washing three times with DPBS, the cells were incubated with100 μg/mL G4-sgc8-NMOFs in culture medium containing 5% FBS for 4 h. After incubation, cells were washed three times with 1 mL of DPBS and subjected to confocal microscopy imaging. For control cells, Ramos cells (1×10^6) were washed three times with DPBS buffer, and then incubated with 100 μg/mL G4-sgc8-NMOFs in culture medium containing 5% FBS for 4 h. After centrifugation, cells were washed with DPBS several times, suspended in DPBS buffer, and then subjected to confocal microscopy imaging.

Singlet oxygen detection

Singlet oxygen sensor green (SOSG) was employed to evaluate the singlet oxygen generation (SOG) by mixing 100 μg/mL TMPyP4-G4-sgc8-NMOFs nanosystem at a concentration of 2.0 μM with 50% D_2O as the solvent using 405 nm laser (2W/cm^2), white light (2.82 W/cm^2) and 660 nm laser irradiation (2 W/cm^2) for different periods of time. SOSG fluorescence was obtained with an excitation wavelength of 494 nm and an emission wavelength of 525 nm. The SOG of samples was quantified by comparing the SOSG fluorescence enhancement with the background.

In vitro toxicity experiments

HeLa cells were first seeded in a 96-well plate at a density of 4×10^3 cells per well and incubated for 24 h. After removing the culture medium, cells were incubated with different concentrations (0.5-5 μM) of TMPyP4, TMPyP4-G4-sgc8, TMPyP4-G4-lib-NMOFs, TMPyP4-G4-sgc8-NMOFs at 37 °C for 4 h. CEM and Ramos cells were seeded in 96-well plates at a density of 4×10^5 cells per well and incubated with different concentrations of TMPyP4, TMPyP4-G4-sgc8, TMPyP4-G4-lib-NMOFs and TMPyP4-G4-sgc8-NMOFs at 37 °C for 4 h. Then, the culture medium was replaced with 200 μL of fresh culture medium. For PDT, cells were irradiated for 2 h with white light at an irradiance of 2.82 W/cm^2 with a wavelength range of 400 to 700 nm. After 48 h incubation, the cell medium was replaced with 120 μL of fresh culture medium and 20 μL of MTS solution. After 30 min incubation, therapeutic efficacy of PDT on different cell lines was assayed by measuring the absorbance at 490 nm.

In vivo PDT treatment

Mice bearing HeLa tumors were randomized into 6 groups (4 mice/group), including PBS group, G4-sgc8-NMOFs group, free TMPyP4 group, TMPyP4-G4-lib-NMOFs group, TMPyP4-G4-sgc8 group and TMPyP4-G4-sgc8-NMOFs group. For PDT treatment, 50 μL of 2 mg/mL G4-sgc8-NMOFs, 50 μL of 100 μM free TMPyP4, 50 μL of 2 mg/mL TMPyP4-G4-lib-NMOFs, 50 μL of 100 μM of TMPyP4-G4-sgc8 or 50 μL of 2 mg/mL TMPyP4-G4-sgc8-NMOFs (corresponding to 100 μM TMPyP4) was intratumorally injected into the tumor-bearing mice. The tumors of all groups were irradiated for 30 min at 2 h post-injection with a xenon lamp (CEL-HXUV300) with an irradiance of 2 W/cm^2 and an optical filter of 660 nm (the irradiance specified refers to before filtering at 660 nm). 5 days later, mice were again subjected to laser irradiation for 30 min, 2 h after further injection as mentioned above. Tumor growth was monitored over 16 days after PDT treatment. Tumor size was monitored with a digital caliper every day and tumor volume was calculated as volume =A×B^2/2, where A is the longer diameter and B is the shorter diameter. The body weights of all mice were measured by caliper every other day after the treatment.

Histological staining

After PDT for 16 days, tumors, liver and kidney were collected from tumor-bearing mice. Tissues were embedded in OCT solution and frozen at -80 °C. Haematoxylin and eosin (H&E) staining was examined with the panoramic MIDI (3D Hi-tech Ltd, Budapest, Hungary).

Abbreviations

PDT: photodynamic therapy; NMOFs: nanoscale metal-organic frameworks; TMPyP4: 5, 10, 15, 20-tetrakis (1-methylpyridinium-4-yl) porphyrin; G4: G-quadruplex; MOFs: Metal-organic frameworks; FITC: fluorescein; EPR: enhanced permeability and retention; Ce6: chlorin e6; ROS: reactive oxygen species; H_2BDC: terephthalic acid; DMF: N, N-dimethylformamide; TEM: transmission electron microscopy; DLS: dynamic light scattering; XPS: X-ray photoelectron spectroscopy; PXRD: powder X-ray diffraction; PTK7: protein tyrosine kinase 7; BET: Brunauer-Emmett-Teller; BJH: Barret-Joyner-Halenda; FTIR: fourier-transform infrared; CD: circular dichroism; SOG: singlet oxygen generation; SOSG: singlet oxygen sensor green; MTS: 3-(4, 5-dimethylthiazol-2-yl)-5-(3-carboxymethoxyphenyl)-2-(4-sulfophenyl)-2-H-tetrazolium; FBS: fetal bovine serum; DPBS: dulbecco's phosphate-buffered saline.

Supplementary Material

Supplementary figures and table.
http://www.thno.org/v08p4332s1.pdf

Acknowledgments

This work was supported by National Natural Science Foundation of China (21605038, 21325520, 21327009, 31701249, 31601125), China Postdoctoral Science Foundation (2016M602245), the Key scientific research project of higher education of the Henan province (16A150013) and the key point research and invention program of Hunan province (2017DK2011).

Author Contributions

H.M.M. and X.X.H. contributed equally to this work. We sincerely appreciate Ms. Hailan Kuai and Mr. Alexander Nti Kani for their kind help with manuscript preparation. The manuscript was written with contributions from all authors. All authors have

given approval to the final version of the manuscript.

Competing Interests

The authors have declared that no competing interest exists.

References

1. Rcooa JD, Liu D, Lin W. Nanoscale metal-organic frameworks for biomedical imaging and drug delivery. Acc Chem Res. 2011; 44: 957-68.
2. Kreno LE, Leong K, Farha OK, Allendorf M, Duyne RPV, Hupp JT. Metal-organic framework materials as chemical sensors. Chem Rev. 2012; 112: 1105-25.
3. Bai Y, Dou Y, Xie LH, Rutledge W, Li JR, Zhou HC. Zr-based metal-organic frameworks: design, synthesis, structure, and applications. Chem Soc Rev. 2016; 47: 2327-67.
4. Morris W, Briley WE, Auyeung E, Cabezas MD, Mirkin CA. Nucleic acid–metal organic framework (MOF) nanoparticle conjugates. J Am Chem Soc. 2014; 136: 7261-4.
5. Cavka JH, Jakobsen S, Olsbye U, Guillou N, Lamberti C, Bordiga S, et al. A new zirconium inorganic building brick forming metal organic frameworks with exceptional stability. J Am Chem Soc. 2008; 130: 13850-1.
6. He C, Lu K, Lin W. Nanoscale metal-organic frameworks for real-time intracellular pH sensing in live cells. J Am Chem Soc. 2014; 136: 12253-6.
7. He C, Lu K, Lin D, Lin W. Nanoscale metal-organic frameworks for the co-delivery of cisplatin and pooled siRNAs to enhance therapeutic efficacy in drug-resistant ovarian cancer cells. J Am Chem Soc. 2014; 136: 5181-84.
8. Zhu X, Gu J, Wang Y, Li B, Li Y, Zhao W, et al. Inherent anchorages in UiO-66 nanoparticles for efficient capture of alendronate and its mediated release. Chem Comm. 2014; 50: 8779-82.
9. Iyer AK, Khaled G, Fang J, Maeda H. Exploiting the enhanced permeability and retention effect for tumor targeting. Drug Discov Today. 2006; 11: 812-8.
10. Kobayashi H, Watanabe R, Choyke PL. Improving conventional enhanced permeability and retention (EPR) effects; what is the appropriate target? Theranostics. 2014; 4: 81-9.
11. Park J, Jiang Q, Feng D, Mao L, Zhou HC. Size-controlled synthesis of porphyrinic metal-organic framework and functionalization for targeted photodynamic therapy. J Am Chem Soc. 2016; 138: 3518-25.
12. Zhang L, Lei J, Ma F, Ling P, Liu J, Ju H. A porphyrin photosensitized metal-organic framework for cancer cell apoptosis and caspase responsive theranostics. Chem Comm. 2015; 51: 10831-4.
13. Ellington AD, Szostak JW. In vitro selection of RNA molecules that bind specific ligands. Nature. 1990; 346: 818-22.
14. Tuerk C, Gold L. Systematic evolution of ligands by exponential enrichment: RNA ligands to bacteriophage T4 DNA polymerase. Science. 1990; 249: 505-10.
15. Meng HM, Liu H, Kuai H, Peng R, Mo L, Zhang XB. Aptamer-integrated DNA nanostructures for biosensing, bioimaging and cancer therapy. Chem Soc Rev. 2016; 45: 2583-2602.
16. Ma H, Liu J, Ali MM, Mahmood MA, Labanieh L, Lu M, et al. Nucleic acid aptamers in cancer research, diagnosis and therapy. Chem Soc Rev. 2015; 44: 1240-56.
17. Iliuk AB, Hu L, Tao WA, Chem A. Aptamer in bioanalytical applications. Anal Chem. 2011; 83: 4440-52.
18. Queffélec C, Petit M, Janvier P, Knight DA, Bujoli B. Surface modification using phosphonic acids and esters. Chem Rev. 2012; 112: 3777-807.
19. Nonglaton G, Benitez IO, Guisle I, Pipelier M, Léger J, Dubreuil D, et al. New approach to oligonucleotide microarrays using zirconium phosphonate-modified surfaces. J Am Chem Soc. 2004; 126: 1497-502.
20. Wang S, McGuirk C. M, Ross MB, Wang S, Chen P, Xing H, et al. General and direct method for preparing oligonucleotide-functionalized metal-organic framework nanoparticles. J Am Chem Soc. 2017; 139: 9827-30.
21. Schreurs TJL, Jacobs I, Nicolay K, Prompers JJ, Strijkers GJ. Detection of treatment success after photodynamic therapy using dynamic contrast-enhanced magnetic resonance imaging. Theranostics. 2017; 7: 4643-57.
22. Han D, Zhu G, Wu C, Zhu Z, Chen T, Zhang X, et al. Engineering a cell-surface aptamer circuit for targeted and amplified photodynamic cancer therapy. ACS Nano. 2013; 7: 2312-19.
23. Liang R, Tian R, Ma L, Zhang L, Hu Y, Wang J, et al. A supermolecular photosensitizer with excellent anticancer performance in photodynamic therapy. Adv Funct Mater. 2014; 24: 3144-51.
24. Zhou L-L, Guan Q, Li Y-A, Zhou Y, Xin Y-B, Dong Y-B. One-pot synthetic approach toward porphyrinatozinc and heavy-atom involved Zr-NMOF and its application in photodynamic therapy. Inorg Chem. 2018; 57: 3169-76.
25. Fan H, Yan G, Zhao Z, Hu X, Zhang W, Liu H, et al. A smart photosensitizer-manganese dioxide nanosystem for enhanced photodynamic therapy by reducing glutathione levels in cancer cells. Angew Chem Int Ed. 2016; 55: 5477-82.
26. Shen L, Huang Y, Chen D, Qiu F, Ma C, Jin X, et al. pH-Responsive aerobic nanoparticles for effective photodynamic therapy. Theranostics. 2017; 7: 4537-50.
27. Shieh YA, Yang SJ, Wei MF, Shieh MJ. Aptamer-based tumor-targeted drug delivery for photodynamic therapy. ACS Nano. 2010; 4: 1433-42.
28. Yuan Q, Wu Y, Wang J, Lu D, Zhao Z, Liu T, et al. Targeted bioimaging and photodynamic therapy nanoplatform using an aptamer-guided G-quadruplex DNA carrier and near-infrared light. Angew Chem Int Ed. 2013; 125: 13965-9.
29. Wang N, Zhao Z, Lv Y, Fan H, Bai H, Meng H, et al. Gold nanorod-photosensitizer conjugate with extracellular pH-driven tumor targeting ability for photothermal/photodynamic therapy. Nano Res. 2014; 7: 1291-301.
30. Haq I, Trent JO, Chowdhry BZ, Jenkins TC. Intercalative G-tetraplex stabilization of telomeric DNA by a cationic porphyrin. J Am Chem Soc. 1999; 121:1768-1779.

Author Biography

Hong-Min Meng graduated with her BS in 2010 and PhD in 2015, both from the Department of Chemistry, Hunan University. She has been an assistant professor in the Department of College of Chemistry and Molecular Engineering at Zhengzhou University since 2017. Her research interests include constructing novel functional nucleic acid-conjugated nanostructures for bioassays, bioimaging and drug delivery.

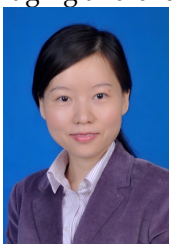

Xiao-Xiao Hu graduated with her PhD in 2010 from Texas A&M Health Science Center, USA. Her research interests include cell-SELEX, bioassays and bioimaging of novel functional aptamers.

Ge-Zhi Kong received her BS from Hunan University in 2015. Currently, she is a PhD candidate in Analytical Chemistry in the College of Chemistry and Chemical Engineering at Hunan University. Her current research interests include the application of DNA nanotechnology to cancer therapy.

Chan Yang received her BS from Hunan University in 2014. She is currently a PhD candidate under the supervisor of Professor Xiaobing Zhang in the Department of Chemistry at Hunan University. Her current research interests include aptamer-integrated nanomaterials and their applications in biosensing, bioimaging and cancer therapy.

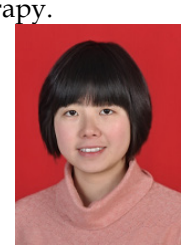

Ting Fu, an engineer, graduated with her PhD in 2017 from Hunan University. Her research is mainly focused on the design and application of nucleic acid probes.

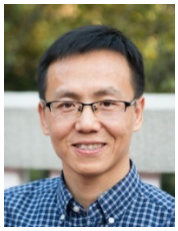

Zhao-Hui Li received his PhD degree in the State Key Laboratory of Chemo/Bio Sensing and Chemometrics at Hunan University in 2007. He did his postdoctoral training in the Walt Group at Tufts University from 2007 to 2009 and in Pacific Northwest National Laboratory from 2009 to 2011. At present, he is a full professor at Zhengzhou University. His research interests mainly focus on nanomaterial preparation and their applications in chemo/biosensing.

Xiao-Bing Zhang is a professor in the Department of Chemistry at Hunan University. He completed his BS in 1993 and PhD in 2001, both in Chemistry from Hunan University. He worked at the Ecole Normale Superieure de Lyon (France) and the Royal Institute of Technology (Sweden) as a postdoctoral fellow from 2003 to 2005. He served as an invited professor at ENS de Lyon in 2008 and as a visiting professor at the University of Illinois at Urbana-Champaign in 2009. Professor Zhang's research interests concern fluorescent chemosensors and functional DNA-based biosensors.